Journal of High Energy Physics, Gravitation and Cosmology, 2026, 12(4), 2309-2330
https://www.scirp.org/journal/jhepgc
ISSN Online: 2380-4335
ISSN Print: 2380-4327

Cosmological and Tokamak Signatures of GW and Gravitons

Andrew W. Beckwith[1], Fangyu Li[1], Gary V. Stephenson[2]

[1]Department of Physics, Chongqing University, Chongqing, China
[2]Seculine Consulting, Potomac, MD, USA
Email: rwill9955b@gmail.com

How to cite this paper: Beckwith, A.W., Li, F.Y. and Stephenson, G.V. (2026) Cosmological and Tokamak Signatures of GW and Gravitons. *Journal of High Energy Physics, Gravitation and Cosmology*, **12**, 2309-2330.
https://doi.org/10.4236/jhepgc.2026.124117

Received: July 23, 2026
Accepted: October 18, 2026
Published: October 21, 2026

Copyright © 2026 by author(s) and Scientific Research Publishing Inc.
This work is licensed under the Creative Commons Attribution International License (CC BY 4.0).
http://creativecommons.org/licenses/by/4.0/
Open Access

Abstract

First, we consider the cosmological geometry of toroidal space, as given in earlier papers. Secondly, we explore how to simulate this toroidal geometry and the emissions thereof using Tokamak GW experimental signatures, albeit in a scaled-down manner. Thirdly, we explore the sensitivity of a HFGW (High Frequency Gravitational Wave) detection device, as given by Pro. Fangyu Li of Chongqing University, and the detection of Tokamak plasma-created GW (Gravitational wave) strain values as low as 10^{-26} in lieu of GW (Gravitational wave) frequencies as high as 60 GHz (60 Gigahertz). This paper is intended to be a preliminary planning document as to how to extend the design concepts given in ITER and other advanced Tokamak generators as to GW (Gravitational wave) development. Appendix A in particular allows foundational issues as to Tokamak detection to be built up as a way to enrich engagement in the basics of GW detection and Gravitons.

Keywords

Torsion, Entanglement, Initial GW Frequencies, HUP (Heisenberg Uncertainty Principle), Black Holes

1. Introduction

This is the geometry which is embedded in both the Tokamak and also the cosmology.

See references [1]-[6] for what we will be reviewing.

Figure 1, taken from reference [1], is almost complete except that we lack the 3-dimensional Tokamak as an approximation of a torus explicitly embedded in the Ekpyrotic model in a time-dependent sense.

In a word, we are counting on the fidelity of toroidal geometry in the early uni-

verse with the problem of Tokamak generation of GW and Gravitons. *i.e.*, see the connection of Figure 1 with the Tokamak as given here.

Set in this Figure 2, Figure 2 has content taken from [1], which is almost complete except that we lack the 3-dimensional Tokamak as an approximation of a torus explicitly embedded in the Ekpyrotic model in a time-dependent sense.

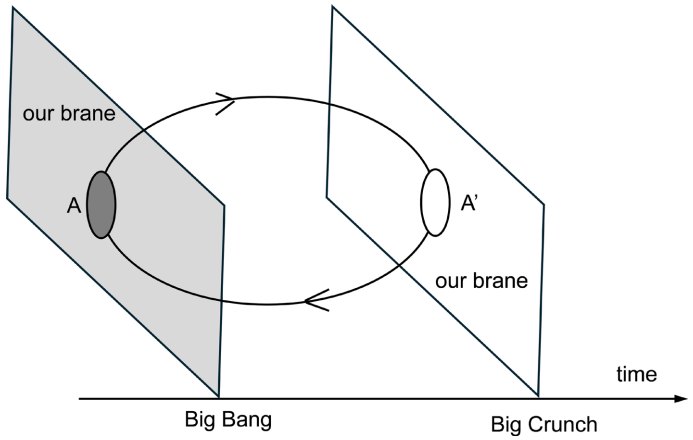


Figure 1. Our Brane in the Ekpyrotic model. By identifying A with A' we obtain a torus.

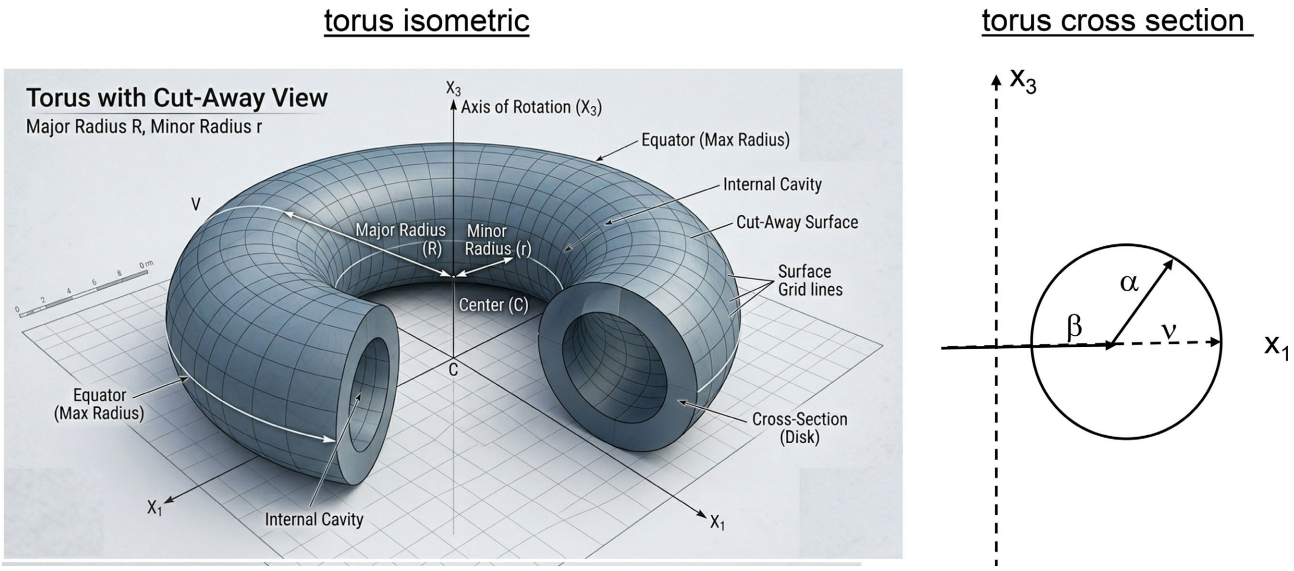


Figure 2. Geometry of the Murzdzek Toroid and coordinates used in the torus. The position of a point on the torus cross section is in coordinates (α, β, and υ).

In this section, we will be examining the Murzdzek Toroid while considering its intersection with cosmology.

In order to do this, we will do the following, namely, look at [1]-[4] for guidance.

Our Figure 2 discussion is more on the geometry of the Murzdzek Toroid [1] [4].

In Figure 2, we use the following coordinates from [1] [4].

Here, we do this in Cartesian coordinates:

$$\begin{aligned} x_1 &= (\beta + \alpha\cos v)\cdot\cos\phi \\ x_2 &= (\beta + \alpha\cos v)\cdot\sin\phi \\ x_3 &= \alpha\sin v \end{aligned} \tag{1}$$

Here, this is for the following surface equation in Cartesian coordinates [1] [4].

$$\left(\beta - \sqrt{x_1^2 + x_2^2}\right)^2 + x_3^2 = \alpha^2 \tag{2}$$

Also, we will set from **Figure 2**, as well as

$$\begin{aligned} \Re &= R \\ \theta &= \vartheta \end{aligned} \tag{3}$$

Furthermore, this will be if we specify a "Toroidal universe radius" as given [4] by setting

$$\Re\sin\Theta = x_1 \tag{4}$$

Note that, for making our notation consistent, $\Re = R$ in **Figure 2**, and we do this so our *R*, which we relabeled, is NOT confused with the Ricci scalar.

This assumes x_1 has ϕ set to zero, and Θ is the angle of a straight line $\Re$ with respect to the drawn axis from x_1 equals zero in **Figure 2** to the surface of the donut in **Figure 2**. Which we call $\Re$.

So, then we have the line element as given by

$$\mathrm{d}s^2 = -(\beta + \alpha\cos v)^2\,\mathrm{d}\phi^2 + \alpha^2\mathrm{d}v^2 \tag{5}$$

In doing this, using [4] again, we refer to the only non-zero Riemannian tensor given as

$$R_{1212} = \alpha\beta\cos v + \alpha^2\cos^2 v \tag{6}$$

Then, the only non-zero Ricci tensor components of the toroid are specified as [4]

$$\begin{aligned} R_{11} &= -\frac{(\beta + \alpha\cos\phi)\cdot\cos\phi}{\alpha} \\ R_{22} &= -\frac{\alpha\cos\phi}{(\beta + \alpha\cos\phi)} \end{aligned} \tag{7}$$

This is extremely important to what we do next, because it means

$$R_{00} = 0 \tag{8}$$

In doing so, effectively in the line element as given in Equation (4) we have that

$$g_{00} = 0 \tag{9}$$

This Equation (8) means then that we would have $T_{00} = 0$, which makes connection to the Space-time geometry next to impossible, this way.

We will still be observing Equation (8), but we wish to embed the Equation (5) line element in a setting where we have $g_{00} = 1$, which is crucial to using $T_{00} \neq 0$. *i.e.*, a non-zero energy density term in our physics comparison between two Ricci scalar terms, for getting $T_{00} \neq 0$, and in doing so, we are looking at the [1] [2] Toroidal case as given by the line element Equation (5) as [2]

$$R_s = -\frac{2\cos v}{\alpha\left(\beta + \alpha\cos v\right)} \tag{10}$$

This is part and parcel of **Figure 2**. And this is also in [4] as well.

Here below is the basics of [1] put in which does NOT include in a time component in terms of a Toroidal geometry. It does NOT include Tokamak geometry directly. This is from [1] in terms of Branes, using references [1] and [2] in terms of Brane geometry. See page 3 of [1] for where this came from.

Note that there are very abstract definitions of Toroidal geometry and quantization in 2 + 1 geometry, as seen in [5] on page 54, which refer to Toroid Moduli in 2 + 1 geometry in what is called Teichmuller space. This leads to a very strange metric given in Page 55, Formula (3.74) of reference [5].

The motivation of the Teichmuller space is to come up with a constant Hamiltonian, which appears good if you want invariance laws. The downside is that in the Teichmuller space, when the Hamiltonian is CONSTANT, we have zero MOMENTUM.

So strange topological constructions do not rescue us. *i.e.*, if we wish for a linkage to space-time geometry which MAY be proportional to Tokamaks, plus a time component, we need to do better. That is what our article is about.

So let us dive into this situation.

A quote from [1] is included as **Figure 2**, and below it is included in time, but it does not conform to the geometry inherent to the Tokamak, leaving us with having the geometry of the Tokamak mapped right back in later after this discussion.

The Brane embedding, as given, does NOT have a direct linkage to 3-dimensional tokamaks.

In doing this, I wish to make a special word of thanks for all this referenced work.

I sincerely wish to praise [4] for, without an explicit time dependence, working on and giving a description of a Toroidal Universe. So I will briefly outline their program, and yes, it is excellent. However, it DOES NOT allow for incorporating particle production, and to have Gravitons produced, one needs a TIME element worked in.

First, let us go back to what was brought up in [4], and it is ALMOST complete, except they keep people away from a time component.

What is done, also by rewriting Equation (1) in spherical coordinates, is that [2] re-images the radii of the Toroidal geometry to obey the following quadratic Equation for the purported radii $\Re$ of the mini-Universe, and this is in fidelity with **Figure 2** above.

$$\Re^2 - 2\Re\beta\sin\Theta + \beta^2 - \alpha^2 = 0 \tag{11}$$

whereas, we have one key piece of mathematics of space-time geometry to consider, namely the issues brought up in [6], which are, in this case, future project-related.

In doing so, we establish a relationship between n and initial spatial regions of Planckian space, which we can write as given in the following quantity as given in

[2] [3]; [7] that, for a huge initial degree of freedom value of $g_* \approx 100$ for pre-Planckian to Planckian transitions showing large quantum number values so that the correspondence principle in cosmology would hold would be to have using energy as given in *E*.

$$n^2\left(\text{quantum number}\right)=\frac{2\cdot V_{\text{space volume}}\cdot m_g\left(1.66\times\sqrt{g_*}\cdot T_{\text{max temperature}}^2\right)^2}{\pi^2\hbar^2} \tag{12}$$

We should before proceeding also note that we would also be utilizing having [1] [2] [7] $\Delta E\equiv\frac{d\left(\dim\right)}{2}\cdot k_B\cdot T_{\text{universe}}$ so that we have

$$n^2\left(\text{quantum number}\right)\approx\frac{2d\left(\dim\right)\cdot V_{\text{space volume}}m_g\cdot\left(R_{\text{radius well}}\right)^2}{\pi^2\hbar^2} \tag{13}$$

where we are assuming having an almost one-to-one connection between g_* and $d\left(\dim\right)$

$$\rho=\frac{E\left(\text{cylindrical well energy}\right)}{V_{\text{volume}}}=\frac{n^2\left(\text{quantum number}\right)\cdot\pi^2\hbar^2}{V_{\text{volume}}\cdot m_g\cdot\left(r_{\text{radius well}}\right)^2} \tag{14}$$

For there to be an equality, which would be a necessary condition for having a correspondence principle in Cosmology, *i.e.*, to have quantum effects for high numbers, *i.e.*, $n^2_{\text{quantum number}}\gg 1$, one would likely have, even if we state g_* is a degree of freedom, that the stated dimensional values of inputs into a very large value for $d_{\dim}$ for inputs into the pre-Planckian state, prior to emergence into Planckian cosmology conditions, would have to be an extremely large number. *i.e.*, we would be looking for conditions in the pre-Planckian spacetime for which $n^2_{\text{quantum number}}\gg 1$ due to an enormous value for $d_{\dim}$.

Having said that, we will also use the following for black holes, numbered as *N*, as opposed to quantum number n.

We begin first with a BEC condensate given by [7]-[10] as to BEC treatment of black holes, and entropy.

$$\begin{aligned}
m &\approx \frac{M_P}{\sqrt{N_{\text{gravitions}}}}\\
M_{BH} &\approx \sqrt{N_{\text{gravitions}}}\cdot M_P\\
R_{BH} &\approx \sqrt{N_{\text{gravitions}}}\cdot l_P\\
S_{BH} &\approx k_B\cdot N_{\text{gravitions}}\\
T_{BH} &\approx \frac{T_P}{\sqrt{N_{\text{gravitions}}}}
\end{aligned} \tag{15}$$

This will lead to the following, as in [7]-[10], for individual black holes.

$$S_{BH}\propto 2n\cdot\log 2-\frac{3}{2}\cdot\log\left(n\right)\propto k_B N_{\text{Gravitons}} \tag{16}$$

We assert that the quantum number n given above would have to tie into Equa-

tion (13), and that we can consider, for individual black holes, a very complicated by the following value of

$$n^2\left(\text{quantum number}\right)=\frac{2\cdot V_{\text{space volume}}\cdot m_g\left(1.66\times\sqrt{g_*}\cdot T^2_{\text{max temperature}}\right)^2}{\pi^2\hbar^2} \tag{17}$$

This quantum number n would be relevant to graviton production as given by Equation (15) and Equation (16). Furthermore, we have that there is a way to present the Radii of the Toroid given in **Figure 2**, which is seen in the quadratic equation of Equation (11). In doing so, we have that there is also an additional way to give a relationship between the wavelength of the GW in the early universe and that of when instability appears in early universe wavefunction data. From Guth [11]

$$\lambda^*=\frac{2\pi}{\sqrt{-\frac{\partial^2\tilde{V}}{\partial\tilde{\phi}^2}\left(\tilde{\phi}_0 t\right)}} \tag{18}$$

This is the early universe wavelength of inflation where we get use of an inflaton potential

$$\begin{aligned} &a\approx a_{\min}t^{\gamma}\\ &\Leftrightarrow\phi\approx\sqrt{\frac{\gamma}{4\pi G}}\cdot\ln\left\{\sqrt{\frac{8\pi G V_0}{\gamma\cdot(3\gamma-1)}}\cdot t\right\}\\ &\Leftrightarrow V\approx V_0\cdot\exp\left\{-\sqrt{\frac{16\pi G}{\gamma}}\cdot\phi(t)\right\}\end{aligned} \tag{19}$$

Notice the fact that Equation (18) has a negative sign. If we call $\tau=it$ for Euclidean time and use Equation (19), we will obtain

$$\lambda^*=\frac{2\pi}{\sqrt{-\frac{\partial^2\tilde{V}}{\partial\tilde{\phi}^2}\left(\tilde{\phi}_0 t\right)}}=\frac{\sqrt{2}\pi\cdot\tau}{\sqrt{\gamma\cdot(3\gamma-1)}} \tag{20}$$

This will be useful in making an order of comparison between the time of instability of early universe GW, and time and what is observed in the Stevenson interpretation of Tokamak generation of GW and Graviton signals.

2. Conclusions: What We Can Do for Experimental Verification

Appendix A gives us a way of using tokamak plasmas to generate a strain value as high as 10^{-26}, which is absolutely essential for HFGW detection, and it is new work which is seen here for the first time. This is largely the work of Gary Stephenson, who is one of the authors of this document.

Appendix B establishes a way to ascertain where the initial energy of the Universe comes from, and it is important because we are making a linkage between the early universe and Tokamak geometry. We use ideas summarized by Andrew Beckwith as to energy flux here.

Appendix C is the groundbreaking work by Fangyu Li, who is the creator and author of this HFGW detection device technology, which Andrew Beckwith and Gary Stephenson have been privileged to have enlightened discussions with over the last decade of interaction with Chongqing University.

We wish to dedicate this paper to Dr. Robert Baker, who courageously, over two decades, set the standards of inquiry as to HFGW in spite of many setbacks. Dr. Baker is responsible for inspiring the implementation of many of the developments seen in this document, and we salute him for his steadfast determination in decades of endeavor. Bob, all of us salute you!

Finally, and not least, Eric Davis deserves a sincere thank you for, in 2007, hoisting the introduction of HFGW technology to many of the HFGW team including Gary Stephenson, and Clive Woods who benefitted from the roundtable discussions. Thank you, Eric!

A special note as to this device. Recent developments in Korea, in China, and also ITER are raising the bar in terms of 10^{-26} strain GW experimental conditions. We should heed what was said by Fangyu Li that it is optimal for the Li-Baker HFGW detector to be placed as close as possible to the center of a Tokamak, to generate the most effective GW data.

Author Contributions

Prof. Beckwith is the primary author of this paper, and of **Appendix B**. Prof. Fangyu Li is the author of **Appendix C**, and Gary Stephenson is responsible for **Appendix A**.

Conflicts of Interest

The authors declare no conflicts of interest regarding the publication of this paper.

References

[1] Murdzek, R. (2006) Cyclic Universes from Torus Geometry. *Romanian Journal of Physics*, **51**, 997-1001. https://rjp.nipne.ro/2006_51_9-10/0997_1002.pdf

[2] Steinhaxdt, P.J. and Turok, N. (2002) The Cyclic Universe: An Informal Introduction. *Nuclear Physics B—Proceedings Supplements*, **124**, 38-49. https://doi.org/10.1016/s0920-5632(03)02075-9

[3] Khoury, J., Ovrut, B.A., Steinhardt, P.J. and Turok, N. (2001) Ekpyrotic Universe: Colliding Branes and the Origin of the Hot Big Bang. *Physical Review D*, **64**, Article ID: 123522. https://doi.org/10.1103/physrevd.64.123522

[4] Murdzek, R. (2007) The Geometry of the Torus Universe. *International Journal of Modern Physics D*, **16**, 681-686. https://doi.org/10.1142/s0218271807009826

[5] Carlip, S. (2009) Quantum Gravity in 2 + 1 Dimensions. Cambridge University Press.

[6] Guth, A. and Vilikin, A. (2025) On Quantum Creation of a Toroidal Universe. In: Barvinsky, A. and Kamenshchik, A., Eds., Open Issues in Gravitation and Cosmology-Original Contributions, Essays and Recollections in Honor of Alexei Starobinsky, Springer, 23 p. https://arxiv.org/abs/2508.08747

[7] Beckwith, A.W. (2025) Part II. How a Tokamak May Allow GW to Be Duplicated in

Simulated Values, with Torsion Cosmology and Quantum Number *n*, and Cosmological Constant from Relic Black Holes. *Journal of High Energy Physics, Gravitation and Cosmology*, **11**, 737-783. https://doi.org/10.4236/jhepgc.2025.113048

[8] de Sabbata, V. and Sivaram, C. (1991) Torsion, Quantum Effects and the Problem of Cosmological Constant. In: Zichichi, A., de Sabbata, V., and Sanchez, N., Eds., *Gravitation and Modern Cosmology*, Springer, 19-36. https://doi.org/10.1007/978-1-4899-0620-5_4

[9] Beckwith, A.W. (2024) How Torsion as Presented by De Sabbata and Sivaram in Erice 1990 Argument as Modified May Permit Cosmological Constant, and Baseline as to Dark Energy. *Journal of High Energy Physics, Gravitation and Cosmology*, **10**, 138-148. https://doi.org/10.4236/jhepgc.2024.101012

[10] Chavanis, P. (2012) Self-Gravitating Bose-Einstein Condensates. In: Calmet, X., Ed., *Fundamental Theories of Physics*, Springer International Publishing, 151-194. https://doi.org/10.1007/978-3-319-10852-0_6

[11] Blau, S.K. and Guth, A.H. (1987) Inflationary Cosmology. 524-603. https://ui.adsabs.harvard.edu/abs/1987thyg.book..524B

[12] Kim, K., Lee, H., Lee, H.H., Kim, K.M., Kim, H., Lee, J., *et al.* (2025) Vacuum Commissioning and Operation Result after the KSTAR PFC Upgrade. *Fusion Engineering and Design*, **219**, Article 115249. https://doi.org/10.1016/j.fusengdes.2025.115249

[13] Jacquinot, J., Bhatnagar, V.P., Cordey, J.G., Horton, L.D., Start, D.F.H., Barnsley, R., *et al.* (1999) Overview of ITER Physics Deuterium-Tritium Experiments in Jet. *Nuclear Fusion*, **39**, 235-253. https://doi.org/10.1088/0029-5515/39/2/307

[14] Garbet, X., Mantica, P., Angioni, C. (2004) Physics of Transport in Tokamaks. *Plasma Physics and Controlled Fusion*, **46**, B557-B574. https://courses.physics.ucsd.edu/2021/Spring/physics218c/Garbet_General.pdf

[15] Ashtekar, A., Berger, B.K., Isenberg, J. and MacCallum, M. (2015) General Relativity and Gravitation: A Centennial Perspective. Cambridge University Press. https://www.cambridge.org/core/books/general-relativity-and-gravitation/57AFB47FCEB825B190CAB4ABD04BB297

[16] Quadrupole Formula. https://en.wikipedia.org/wiki/Quadrupole_formula

[17] Physical Constant. https://en.wikipedia.org/wiki/Physical_constant

[18] ITER Vacuum Vessel. https://www.iter.org/components?id=0

[19] KSTAR. https://en.wikipedia.org/wiki/KSTAR

[20] ITER. https://en.wikipedia.org/wiki/ITER

[21] Lee, H.Y., Kang, J.S., Wi, H.H., Wang, S.J., Kwak, J.G. and Saito, K. (2021) Power Deposition of H Minority Heating with a New Compact ICRF Antenna in Kstar. *Journal of the Korean Physical Society*, **78**, 1067-1071. https://doi.org/10.1007/s40042-021-00141-y

[22] Photon Energy. https://en.wikipedia.org/wiki/Photon_energy

[23] Jain, R. and Kartikeyan, M.V. (2010) Design of A 60 GHz, 100 kW CW Gyrotron for Plasma Diagnostics: Gds-V.01 Simulations. *Progress In Electromagnetics Research B*, **22**, 379-399. https://doi.org/10.2528/pierb10061508

[24] Ye, X., Wang, Y., Yao, J., Yuan, C., Zhou, Z., Astafiev, A.M., *et al.* (2022) Plasma-enabled Microwave Modulation for Continuous Beam Scanning. *Journal of Physics D: Applied Physics*, **55**, Article 435202. https://doi.org/10.1088/1361-6463/ac8da1

[25] Li, F., Chen, Z. and Yi, Y. (2018) Utilization of Electromagnetic Detector for Selection and Detection of High-Frequency Relic Gravitational Waves.

https://arxiv.org/pdf/gr-qc/0511013v1

[26] Beckwith, A.W. (2026) Pathways to Quantum Cosmology. Scientific Research Publishing. https://doi.org/10.4236/9798895073196

[27] Beckwith, A.W. (2026) What Is a Way to Introduce a Huge Flux of Energy in the Initial Onset of Inflation? *i.e.* Use of Modified Hup and Torsion and a Possible Link to Quantum Number N Meant to Unify Black Holes, and a Quantum Universe. *Journal of High Energy Physics, Gravitation and Cosmology*, **12**, 498-584. https://doi.org/10.4236/jhepgc.2026.121028

[28] Li, F.-Y., Tang, M.-X. and Shi, D.-P. (2003) Electromagnetic Response of a Gaussian Beam to High-Frequency Relic Gravitational Waves in Quintessential Inflationary Models. *Physical Review D*, **67**, Article 104008. https://doi.org/10.1103/PhysRevD.67.104008

[29] Li, F.Y., Baker, R.M.L., Fang, Z.Y., Stephenson, G.V. and Chen, Z.Y. (2008) Perturbative Photon Fluxes Generated by High-Frequency Gravitational Waves and Their Physical Effects. *The European Physical Journal C*, **56**, 407-423. https://doi.org/10.1140/epjc/s10052-008-0656-9

[30] Li, F.Y., Yang, N., Fang, Z.Y., Baker, R.M.L., Stephenson, G.V. and Wen, H. (2009) Signal Photon Flux and Background Noise in a Coupling Electromagnetic Detecting System for High Frequency Gravitational Waves. https://arxiv.org/abs/0909.4118

[31] Clarkson, C. and Seahra, S.S. (2007) A Gravitational Wave Window on Extra Dimensions. *Classical and Quantum Gravity*, **24**, F33-F40. https://doi.org/10.1088/0264-9381/24/9/f01

[32] The LIGO Scientific Collaboration and The Virgo Collaboration (2009) An Upper Limit on the Stochastic Gravitational-Wave Background of Cosmological Origin. *Nature*, **460**, 990-994. https://doi.org/10.1038/nature08278

[33] Gasperini, M. and Veneziano, G. (2003) The Pre-Big Bang Scenario in String Cosmology. *Physics Reports*, **373**, 1-212. https://doi.org/10.1016/s0370-1573(02)00389-7

[34] Giovannini, M. (1999) Production and Detection of Relic Gravitons in Quintessential Inflationary Models. *Physical Review D*, **60**, Article 123511. https://doi.org/10.1103/physrevd.60.123511

[35] Giovannini, M. (2008) Thermal History of the Plasma and High-Frequency Gravitons. https://arxiv.org/abs/0807.4317

[36] Cruise, A.M. (2000) An Electromagnetic Detector for Very-High-Frequency Gravitational Waves. *Classical and Quantum Gravity*, **17**, 2525-2530. https://doi.org/10.1088/0264-9381/17/13/305

[37] Ballantini, R., Bernard, Ph., Calatroni, S., Chiaveri, E., Chincarini, A., Croce, R.P., *et al.* (2005) Microwave Apparatus for Gravitational Waves Observation. https://arxiv.org/abs/gr-qc/0502054

[38] Stephenson, G.V. and Robertson, G.A. (2009) The Standard Quantum Limit for the Li-Baker HFGW Detector. *AIP Conference Proceedings*, **1103**, 542-547. https://doi.org/10.1063/1.3115563

[39] Bisnovatyi-Kogan, G.S. and Rudenko, V.N. (2004) Very High Frequency Gravitational Wave Background in the Universe. *Classical and Quantum Gravity*, **21**, Article 3347. https://doi.org/10.1088/0264-9381/21/14/001

[40] Yariv, A. (1975) Quantum Electronics. 2nd Edition, Wiley.

[41] Woods, R.C., Baker, R.M.L., Li, F.Y., Stephenson, G.V., Davis, E.W. and Beckwith, A. (2010) A New Theoretical Technique for the Measurement of Highfrequency Relic Gravitational Waves. http://vixra.org/abs/1010.0062

[42] Wen, W., Zhou, L., Li, J., Ge, W., Chan, C.T. and Sheng, P. (2002) Subwavelength Photonic Band Gaps from Planar Fractals. *Physical Review Letters*, **89**, Article 223901. https://doi.org/10.1103/physrevlett.89.223901

[43] Zhou, L., Wen, W., Chan, C.T. and Sheng, P. (2003) Reflectivity of Planar Metallic Fractal Patterns. *Applied Physics Letters*, **82**, 1012-1014. https://doi.org/10.1063/1.1553993

[44] Kim, W.-J., Brownell, J.H. and Onofrio, R. (2006) Detectability of Dissipative Motion in Quantum Vacuum via Superradiance. *Physical Review Letters*, **96**, Article 200402. https://doi.org/10.1103/PhysRevLett.96.200402

[45] Yamamoto, K., Tada, M., Kishimoto, Y., Shibata, M., Kominato, K., Ooishi, T., Yamada, S., Saida, T., Funahashi, H., Masaike, A. and Matsuki, S. (2010) The Rydberg-Atom-Cavity Axion Search. https://arxiv.org/abs/hep-ph/0101200

[46] Service, R.F. (2010) Next Wave of Metamaterials Hopes to Fuel the Revolution. *Science*, **327**, 138-139. https://doi.org/10.1126/science.327.5962.138

[47] Krauss, L.M., Dodelson, S. and Meyer, S. (2010) Primordial Gravitational Waves and Cosmology. *Science*, **328**, 989-992. https://doi.org/10.1126/science.1179541

[48] Ni, W.-T., Zhu, J., Wu, X.-P., Chu, G.-B., Yang, B., Gao, J., *et al.* (2002) Mini-ASTROD: Mission Concept. *International Journal of Modern Physics D*, **11**, 1035-1048. https://doi.org/10.1142/S0218271802002542

[49] Conlon, J.P., Copeland, E.J., Hardy, E. and González, N.S. (2026) High-Frequency Gravitational Waves from Superstring Phases in the Early Universe. *Journal of High Energy Physics*, **2026**, Article No. 92. https://doi.org/10.1007/JHEP08(2026)092

[50] Sivaram, C. and Arun, K. (2011) Thermal Gravitational Waves. *The Open Astronomy Journal*, **4**, 65-71. https://doi.org/10.2174/1874381101004010065

Appendix A: Gravitational Wave Emission from Tokamak Plasma—Theoretical Models and Practical Limitations (GW from Tokamak Summary)

This appendix synthesizes technical analyses regarding the generation of gravitational waves (GW) within tokamak nuclear fusion reactors. Based on Einstein's General Theory of Relativity and the Quadrupole Formula, this appendix evaluates the feasibility of using plasma oscillations as a source for GW emission. The primary findings indicate that while gravitational waves are technically emitted by the time-varying mass quadrupole moments of plasma in reactors like KSTAR and ITER, the current magnitudes are profoundly negligible [12] [13].

For the KSTAR tokamak, the emitted power is approximately 1.58×10^{-24} Watts, producing a spacetime strain (h) of roughly 2.97×10^{-39}—a value thousands of times smaller than the Planck length and far beyond any measurable threshold.

However, theoretical scaling suggests that increasing the quadrupole modulation frequency to the GHz range (e.g. 10 to 60 GHz) and increasing the participating plasma mass could significantly elevate the power output, as P_{gw} scales with the sixth power of frequency (f^6). This trade space is explored in this appendix.

A1. Mathematical Framework for Gravitational Radiation

The emission of gravitational waves requires a time-varying mass quadrupole moment. In a tokamak system, this occurs when plasma density concentrations oscillate or rotate in a symmetric quadrupole configuration (e.g., alternating between orthogonal axes).

A1.1. Core Equations

The following formulas define the relationship between plasma parameters and gravitational output:

- **Modulated Mass Fraction (M_{mod}):** The portion of plasma mass undergoing quadrupole modulation [14].

$$M_{mod} = M_{pl} \times \left(\frac{MF_{pl}}{100} \right) \tag{A1}$$

- **Emitted Gravitational Wave Power (P_{gw}) [15]:**

$$P_{gw} = \left(\frac{16\pi^5 G}{5c^5} \right) M_{mod}^2 R^4 F_{pl}^6 \tag{A2}$$

- **Gravitational Wave Strain (h):** The dimensionless metric perturbation experienced by an observer at distance r [16]:

$$h = \left(\frac{2\pi^2 G}{c^4 r} \right) M_{mod} R^2 F_{pl}^2 \tag{A3}$$

A1.2. Key Physical Variables [17]

- G: Gravitational Constant (~6.6743×10^{-11} $m^3 \cdot kg^{-1} \cdot s^{-2}$).
- c: Speed of Light (~2.998×10^8 m/s).

- ***R***: Major radius of the tokamak torus.
- F_{pl}: Quadrupole modulation frequency (Hertz).

A2. Scenario Analysis and Scaling

The power of an emitted gravitational wave is highly sensitive to the modulation frequency. Because P_{gw} scales with F_{pl}^{6}, moving from MHD (Magnetohydrodynamic) frequencies to microwave frequencies drastically changes the theoretical output.

A2.1. Comparative Scenarios

The following table outlines data from various theoretical scenarios based on an ITER-scale radius ($R = 6.2$ meters) [18] with an assumed observer distance of 5.0 meters. Lesser distances may be unrealistic given the instrumentation size needed to support tokamak operations. See Table A1 for a list of scenarios explored so far. The mass of a hypothetical dense plasma was assumed to be 2 grams.

Table A1. Tokamak generated GW scenarios [19] [20] [A8] [A9].

Scenario Name	Plasma Mass M_{pl} (kg)	Mass Fraction MF_{pl} (%)	Modulated Mass M_{mod} (kg)	Quadrupole Freq F_{pl} (Hz)	GW Power P_{gw} (Watts)	GW Strain h (dim)
MHD Baseline	1.00E−05	30.0%	3.00E−06	1.00E+03	1.13E−39	3.76E−42
1 MHz RF Modulation	1.00E−05	30.0%	3.00E−06	1.00E+06	1.13E−21	3.76E−36
1 GHz Oscillation	1.00E−05	30.0%	3.00E−06	1.00E+09	1.13E−03	3.76E−30
ITER MHD Mode	1.00E−04	50.0%	5.00E−05	1.00E+04	3.13E−31	6.27E−39
Hypothetical Dense Plasma, 1 GHz Case	1.00E−02	80.0%	8.00E−03	1.00E+09	8.02E+03	1.00E−26
Hypothetical Dense Plasma, 60 GHz Case	1.00E−02	80.0%	8.00E−03	6.00E+10	3.74E+14	3.61E−23

A2.2. Frequency Sweep Observations

As shown in Figure A1, the analysis of a fixed mass ($M_{pl} = 1.0 \times 10^{-5}$ kg), strain (h) increases linearly on a log-log scale against frequency, reaching approximately 1.35×10^{-26} at 60 GHz. Thus, it is observed that the frequency dependence of GW generation strongly favors the highest achievable quadrupole plasma stimulation frequencies.

A3. Case Study: KSTAR and Ion Cyclotron Resonance Heating (ICRH)

A critical distinction must be made between the engineering use of the term "quadrupole" in tokamak operations and the physical requirements for gravitational waves.

A3.1. Quadrupole Phasing vs. Mass Quadrupole Moment

In the KSTAR tokamak, Ion Cyclotron Resonance Heating (ICRH) utilizes a four-strap antenna array. Researchers use "quadrupole phasing" to adjust the radio fre-

quency (RF) phases of these straps [21]. This is used for:

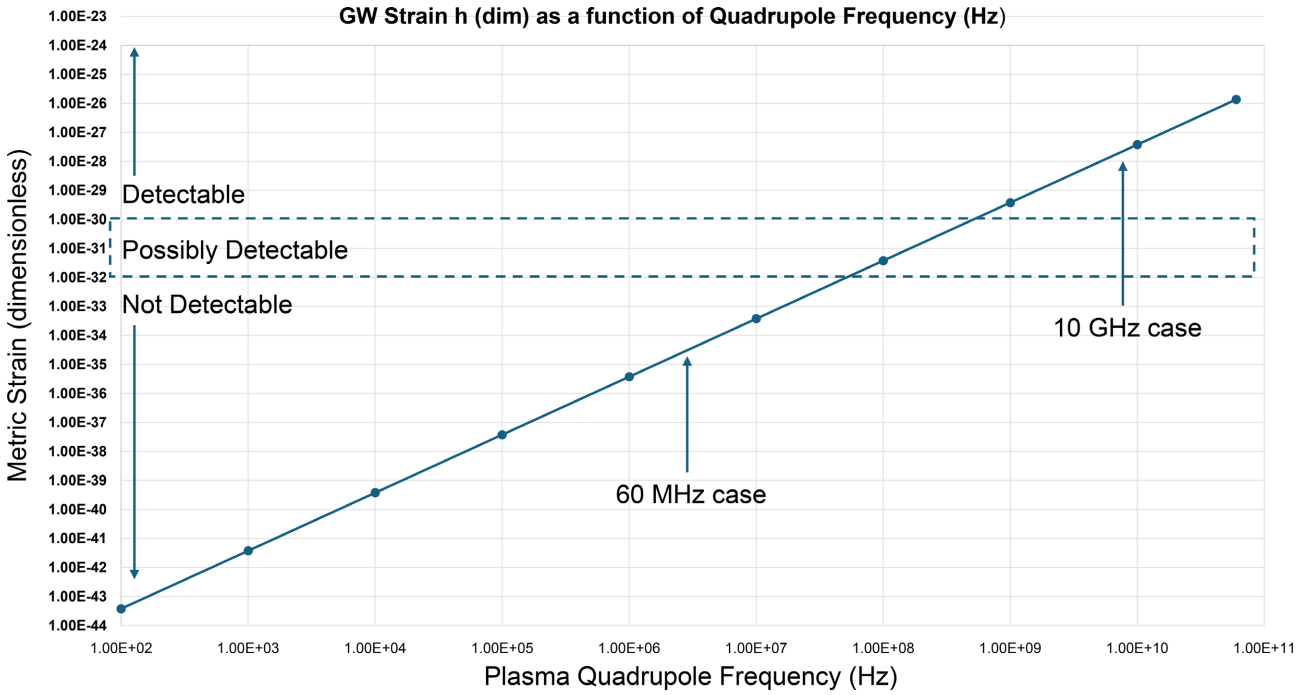


Figure A1. The quadrupole frequency dependence of gravitational wave emissions.

- **Minimizing RF Impurities:** Reducing the sputtering of tungsten from reactor walls.
- **Localized Heating:** Optimizing energy coupling into the deuterium plasma core. While this creates a spatial quadrupole pattern in the electromagnetic field, it does not significantly manipulate the mass properties of the core gas to a degree relevant for GW generation.

A3.2. The Mass Deficit

For a detectable gravitational wave, cosmic-scale masses (e.g., merging black holes) are typically required. KSTAR's total confined deuterium plasma mass is only 1.2 to 6.0 milligrams [19].

- **Static Mass Quadrupole Moment (I_{zz}):** ~1.9×10^{-5} kg m^2.
- **Time-Varying Component (D I):** Induced by ICRH at 30 - 60 MHz, this dynamic mass is estimated at less than 0.1% of the total fuel (10^{-9} kg). The resulting D I is a negligible 10^{-13} to 10^{-11} kg·m^2.

A3.3. Physical Perspective on KSTAR Output

The absolute upper limit of radiated GW power for KSTAR is 1.58×10^{-24} Watts.

- A typical visible light photon carries roughly 3×10^{-19} Joules [22].
- At KSTAR's radiation rate, it would take over two days for the plasma to emit the energy equivalent of a single photon of light in the form of gravitational energy.
- LIGO requires a strain sensitivity h of ~10^{-21} to detect stellar collisions; KSTAR's

strain of ~10^{-39} is eighteen orders of magnitude below this.

A4. Feasibility of High-Frequency (60 GHz) Modulation [23] [24]

To increase GW power, engineers might consider higher modulation frequencies, such as 60 GHz (millimeter-wave regime). However, this introduces plasma physics constraints:

- **Electron Plasma Frequency Cutoff:** In unmagnetized plasma, 60 GHz waves will not propagate and will instead be reflected if the electron density is too high. Effective interaction only occurs if the local plasma frequency is below 60 GHz.
- **Coupling Requirements:** Efficient 60 GHz modulation requires one or more of a number of specific conditions:
  - **Low-density plasma:** Feasible for probing and modulation.
  - **Dense plasma:** Often reflected or attenuated unless specialized near-field or surface-wave coupling is used.
  - **Magnetized plasma:** Can utilize resonant or anisotropic wave physics to bypass standard cutoff limits.
- **Engineering Rule of Thumb:** 60 GHz can modulate a plasma, but many plasmas will not support coherent propagation at this frequency due to collision rates and density parameters.

A5. Conclusions Regarding the Use of Tokamaks for GW Generation

It is generally understood from papers addressing the detection of high-frequency gravitational waves (HFGW) that values of strain h must be within the range of 10^{-32} to 10^{-30} in order to be detectable [25]. Thus, none of the cases representing a repurposing of KSTAR or ITER will have a sufficiently strong strain signal to be detectable.

- **Purpose-built devices:** As noted in **Table A1**, should the plasma mass available for quadrupole modulation be increased from, say, 50 mg to 2 grams, and the quadrupole modulation were to be increased from an RF range of 1 to 60 MHz to a microwave or millimeter range of 10 - 60 GHz, then it is possible to generate a strain signal that may be detectable, should any of the theoretical HFGW sensors be built.
- **Recommended future work:** The design and development of a toroidal microwave dense plasma modulator is beyond the scope of the present appendix. The current appendix scope is limited to developing the requirements of a GW generator purpose-built device. The design of such a device is left to future work.

Appendix B: Obtaining the Initial Energy Flux of the Universe, and Its Magnitude

B1. Deterministic Embedding

As indicated, there are several states in this presentation. First is the idea of using

the HUP from a deterministic embedding in 5 dim, as given in Equation (1), which can be linked to Equation (B1) and Equation (B2), where we have then [26] [27]

$$\begin{aligned} &\left|\mathrm{d}p_{\alpha}\mathrm{d}x^{\alpha}\right| \approx \frac{L}{l}\cdot\frac{h}{c}\cdot\left[\frac{\mathrm{d}l}{l}\right]^{2} \\ &\xrightarrow[\alpha=0]{} \left|\mathrm{d}p_{0}\mathrm{d}x^{0}\right| \simeq \left|\Delta E\Delta t\right| \approx \left(h/a_{\mathrm{init}}^{2}\phi(t)\right) \\ &\Rightarrow \frac{L}{l}\cdot\frac{h}{c}\cdot\left[\frac{\mathrm{d}l}{l}\right]^{2} \approx \left(h/a_{\mathrm{init}}^{2}\phi\left(t_{\mathrm{init}}\right)\right) \end{aligned} \tag{B1}$$

$$\begin{aligned} \sqrt{\Lambda} &= \frac{k_{B}E}{\hbar c S_{\mathrm{entropy}}} \\ S_{\mathrm{entropy}} &= k_{B}N_{\mathrm{particles}} \end{aligned} \tag{B2}$$

The upshot is that we will be changing the cosmological constant from

$$\left(\frac{8\pi G}{3}\right)\cdot\left[-\frac{2\pi G\sigma^{2}}{3c^{4}}\right]+\frac{\Lambda c^{2}}{3}=0 \tag{B3}$$

What we are arguing is that instead, one is seeing, instead

$$\left(\frac{8\pi G}{3}\right)\cdot\left[-\frac{2\pi G\sigma^{2}}{3c^{4}}\right]+\frac{\Lambda_{Pl}c^{2}}{3}\approx 10^{-122}\times\left(\frac{\Lambda_{Pl}c^{2}}{3}\right) \tag{B4}$$

Our timing as to Equation (B4) is to unleash a Planck time interval t about 10^{-43} seconds. As to Equation (B3) versus Equation (B4), the creation of the torsion term is due to a presumed particle spin density of

$$n_{Pl}\approx 10^{98}\ \mathrm{cm}^{-3} \tag{B5}$$

B2. Energy Flux at the Start of Inflation?

Space constraints do not allow us to explain more than this, other than to bring up that the Torsion argument is to buttress the following for energy density, which we give as [26] [27]

$$\begin{aligned} &\rho_{\Lambda}c^{2} = \int_{0}^{E_{\mathrm{Plank}}/c}\frac{4\pi p^{2}\mathrm{d}p}{(2\pi\hbar)^{3}}\cdot\left(\frac{1}{2}\cdot\sqrt{p^{2}c^{2}+m^{2}c^{4}}\right)\approx\frac{\left(3\times10^{19}\ \mathrm{GeV}\right)^{4}}{(2\pi\hbar)^{3}} \\ &\xrightarrow[E_{\mathrm{Plank}}/c\to10^{-30}]{}\frac{\left(2.5\times10^{-11}\ \mathrm{GeV}\right)^{4}}{(2\pi\hbar)^{3}} \end{aligned} \tag{B6}$$

This means shifting the energy level of Equation (B5) with respect to black holes, and that the quantum number comes from [26] [27]

$$\begin{aligned} M_{BH} &\approx \sqrt{N_{\mathrm{gravitons}}}M_{P} \\ \Rightarrow \left(1/M_{BH}\right)^{1/2} &\approx \frac{n_{\mathrm{quantum}}}{2}\approx\frac{1}{\left(N_{\mathrm{gravitons}}\right)^{1/4}} \\ \Rightarrow n_{\mathrm{quantum}} &\approx \frac{2}{\left(N_{\mathrm{gravitons}}\right)^{1/4}} \end{aligned} \tag{B7}$$

Finally, this also leads to a huge energy flux; we can write for Potential energy initially [26] [27]

$$V_0 = \left(\sqrt{\frac{v(3v-1)}{8\pi}} + \sqrt{2\cdot(3v-1)} \cdot \frac{a_{\text{init}}^2 \cdot (l_2 - l_1)^2}{l^3(c)\cdot(3\Lambda)^{1/2}} \right)^2 \approx \Delta E \tag{B8}$$

This uses a scale factor we write as $a(t) \approx a_{\text{init}} t^v$ and also a linkage to a 5-dimensional line element, Λ, and time, which we write as [26] [27], as well as Planck time, which we give below in Equation (B10), which is linked to Equation (1) and Equation (B1) as discussed in [27]. This leads to Planck time. Also, we use a 5-dimensional wave number as $K_1 = 1/l$.

$$dS_{5\text{-}d}^2 = \frac{L^2}{l^2} dS_{4\text{-}d}^2 - \frac{L^4}{l^4} dl^2 \tag{B9}$$

$$t = t_{\text{planck}} \to 1 = \sqrt{\frac{v(3v-1)}{8\pi V_0}} + \sqrt{\frac{2\cdot(3v-1)}{V_0}} \cdot \frac{a_{\text{init}}^2 \cdot (l_2 - l_1)^2}{l^3(c)\cdot(3\Lambda)^{1/2}} \tag{B10}$$

Appendix C: The Sensing of High Frequency Gravitational Waves (HFGW) via a 3D Synchro-Resonance (3DSR) Detector

C.1. Introduction

Chinese and the U.S. HFGW research teams have proposed and planned HFGW detection schemes [28]-[30] in the 10^9 to 10^{10} Hz range. The teams believe that an initial target space-time strain sensitivity of $h \sim 10^{-27}$ in the GHz band is realistic, and that the sensitivity could be improved to 10^{-30}. These detectors would therefore also be promising for observations of either HFGWs in brane oscillation models [31] or relic HFGWs in pre-Big Bang models [32] [33] as well as relic HFGW signals from quintessential inflationary models [34] [35].

C.2. HFGW Detection in the GHz to THz Band: Practical Concerns

One must consider the following operational constraints limiting sensitivity:

C.2.1 Operational temperature T (of the detection device) must satisfy the low-temperature condition of $k_B T < \hbar\omega_e$ (k_B is Boltzmann's constant). If a HFGW has a frequency of 3×10^{10} Hz, then T must be less than 1.4 K.

C.2.2 External noise photons must be suppressed and shielded to a fraction of the signal photon count.

C.2.3 The mean free path of the signal photons at low vacuum pressure must be larger than the coherent interaction dimension of the system.

C.2.4 The expected sensitivity cannot fall below the standard quantum limit (SQL).

The present approach is related to HFGW detectors in microwave cavities [36] [37]. The expression of the minimal detectable space-time strain $h_{\min}$ of the cavity detectors is limited by the level of SQL [38] [39] when analyzing HFGWs is

$$h_{\min} \approx \frac{1}{Q}\sqrt{\frac{\hbar\omega_e}{E}} \tag{C1}$$

for coherent HFGW signals and

$$h_{\min} \approx \frac{1}{\sqrt{Q}}\sqrt{\frac{\hbar\omega_e}{E}} \tag{C2}$$

for stochastic HFGWs. In both Equation (C1) and Equation (C2), Q is the quality factor and $\mathcal{E}$ is the total EM energy in a cavity: the greater the contained energy, the less the impact of quantum back action. Equation (C1) and Equation (C2) are general expressions for SQL, including the GW cavity detectors and other EM detectors, e.g., three-dimensional synchro-resonance (3DSR) detection, proposed and planned by China and the U.S. HFGW research teams [28]-[30]. For superconducting cavities, Q can be ~10^{10} to 10^{12} [10]. If $Q = 10^{11}$, $\mathcal{E} = 10$ J and the frequency is 3 × 10^{10} Hz, then one will obtain from Equation (C1) $h_{\min} \sim 10^{-23}$ for the constant-amplitude HFGWs, and Equation (C3) yields $h_{\min} \sim 10^{-18}$ for the stochastic HFGWs. Therefore, we can conclude that advanced cavity detectors could be a promising detection means for HFGWs expected by the brane oscillation models.

On the other hand, the amplitude magnitude of relic HFGWs in the GHz band predicted by cosmological models [32]-[35] would be $h \sim 10^{-29}$ to 10^{-30} or less. The SEMCS would be a promising scheme to detect relic HFGWs only if the contained energy is increased from the $\mathcal{E} = 10$ J level.

C.3. Laboratory Instrument Design Considerations

For the laboratory situation (see **Figure C1**): $B^{(0)} = 3T$, $\Delta L = 6$ m and $\Delta S = 0.3\ \mathrm{m}^2$, if we add a pseudo-plane EM wave (EMW) beam with $p = 10$ W, $v_e = v_g = 2.9$ GHz, which propagates in the same direction as the HFGW, and according to Ref. [30] one finds the background photon flux (BPF) $N_\gamma^{(0)} = 5.3\times10^{24}\ \mathrm{s}^{-1}$, the first-order perturbative photon flux (PPF) $N_\gamma^{(1)} = 1.2\times10^{5}\ \mathrm{s}^{-1}$ and the second-order PPF $N_\gamma^{(2)} = 4.9\times10^{-17}\ \mathrm{s}^{-1}$. We claim that $N_\gamma^{(1)} + N_\gamma^{(2)} \approx N_\gamma^{(1)}$ has HFGW "information".

The problem is that $N_\gamma^{(1)}$ would be overcome by a large BPF noise, thus $N_\gamma^{(1)}$ would be a small fraction of the total photon flux and would be swamped. Thus, we wish to obtain a special EM system for which $N_\gamma^{(1)}$ and $N_\gamma^{(0)}$ have different physical behavior, for instance a different spatial distribution. In practice, the 3DSR detector planned by the HFGW research teams will allow for such a differentiation between $N_\gamma^{(1)}$ and $N_\gamma^{(0)}$ [28]-[30].

C.3.1. The 3DSR Plus Modern Technology: Detection Scheme for the Relic HFGWs in the GHz Band

The 3DSR is a coupling system for a Gaussian-type microwave photon flux, a static magnetic field, and fractal membrane acting as a focusing element [28]-[30].

The general form of the Gaussian beam (GB) of fundamental frequency mode is per [40]:

$$\psi = \frac{\psi_0}{\sqrt{1+(z/f)^2}}\exp\left(-\frac{r^2}{W^2}\right)\exp\left(i\left[k_e z - \omega_e t - \tan^{-1}\frac{z}{f} + \frac{k_e r^2}{2R} + \delta\right]\right) \tag{C3}$$

where $r^2 = x^2 + y^2$, $k_e = \frac{2\pi}{\lambda_e}$, $W = W_0\sqrt{1+\left(\frac{z}{f}\right)^2}$, $R = z + f^2/z$, ψ_0 is the amplitude of the electric (or magnetic) field of the GB, W_0 is the minimum spot radius, R is the curvature radius of the wave front of the GB at z, the z-axis is the symmetrical axis of the GB and the incident GW, δ is a phase factor, and ψ satisfies the Helmholtz equation. It is an important distinction that, unlike plane EM waves, any GB has longitudinal (z direction) photon flux $n_z^{(0)}$, as well as a transverse (radial) photon flux $n_r^{(0)}$. According to the electrodynamics equations in curved space-time, it was shown that [28]-[30]:

All background photon flux BPFs $n^{(0)}$ have the Gaussian decay rate factor $\exp\left(-2r^2/W^2\right)$ due to $n^{(0)} \propto |\psi|^2$, while first-order PPFs $n^{(1)}$ decay by $\exp\left(-r^2/W^2\right)$ due to $n^{(1)} \propto |\psi|$ (see **Figure C1**). Therefore, $n^{(1)}$ and $n^{(0)}$ have similar magnitude at a distance of several spot radii, although $n^{(1)}$ is usually much less than $n^{(0)}$ in other regions. In this case, the resonant effect is sensitive to the frequencies and propagating direction of HFGWs. The resonance condition specifies that transverse PPF $n^{(1)}$ has a maximum value at a longitudinal symmetrical surface of the GB where transverse BPF vanishes. Thus, $n^{(1)}$ is a major fraction of the total transverse photon flux passing through the longitudinal symmetrical surface (see **Figure C2**). Moreover, since $n_x^{(1)}$ and $n_x^{(0)}$ have an opposite propagation direction in $x < 0$, in the 3DSR. This "anti-symmetric" property ensures conservation of total momentum in coherent resonance interactions.

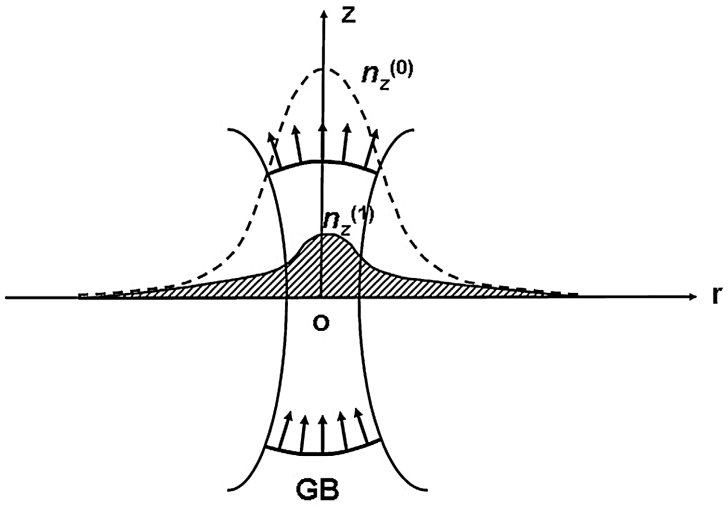


Figure C1. The longitudinal BPF $n_z^{(0)}$ and PPF $n_z^{(1)}$ in the SEMCS, where z-axis is the symmetrical axis of the GB. Here, black lines express the envelope and wavefront of the GB, respectively. The space of $z > 0$ is the outgoing wave region of the GB, and the space of $z < 0$ is the imploding wave region. The BPF, depicted by the dashed line curve $n_z^{(0)}$ decays by the typical Gaussian decay rate $\exp\left(-2r^2/W^2\right)$ at the transverse direction, while the PPF, depicted by the filled curve $n_z^{(1)}$ decays by the factor $\exp\left(-r^2/W^2\right)$ in this direction.

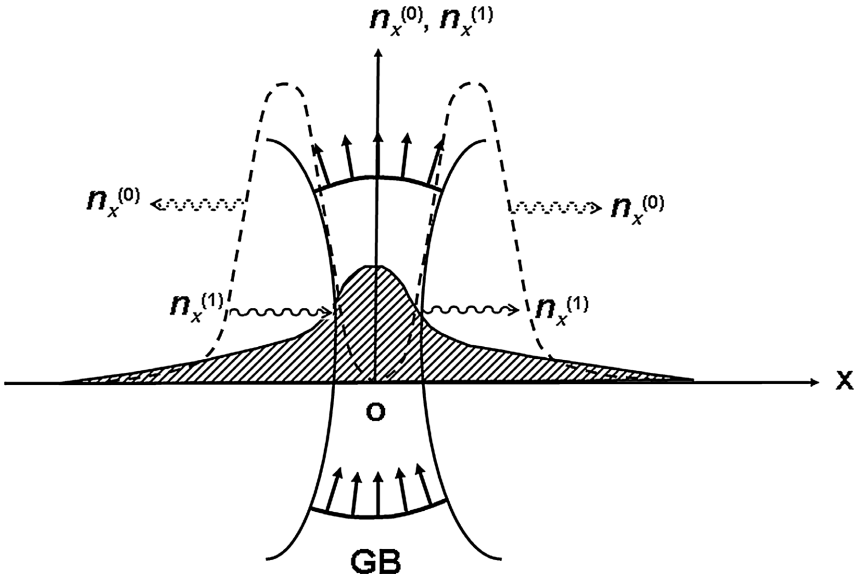


Figure C2. Schematic diagram of the transverse BPF $n_x^{(0)}$ and PPF $n_x^{(1)}$ in the outgoing wave region ($z>0$) of the GB. Unlike **Figure 2**, here $n_x^{(0)}\big|_{x=0}=0$ while $n_x^{(1)}\big|_{x=0}=n_{x\,\max}^{(1)}$. Therefore, the major fraction of the transverse photon fluxes transmitted by the FM lying at the longitudinal symmetrical surface (*yz*-plane)or at the parallel surface very near the *yz* plane would be PPF, depicted by the filled curve $n_x^{(1)}$, and not BPF, depicted by the dashed line $n_x^{(0)}$. The integrated PPF $n_x^{(1)}\Delta t$ can therefore be effectively larger than the integrated background noise photon flux $\sqrt{n_x^{(0)}\Delta t}$ in typical laboratory sampling interval (~10^5 to 10^6 seconds).

C.3.2. Displaying Condition of the Relic HFGWs

Unlike longitudinal photon fluxes (see **Figure C1**), the transverse BPF $n_x^{(0)}$ and PPF $n_x^{(1)}$ have different physical behaviors (see **Figure C2**) [29] [30], including distribution, propagating direction, decay rate, phase, etc. Total transverse noise photon fluxes $N_{x(\text{total})}^{(0)}$ passing through an effective receiving surface ΔS include the transverse background photon flux $N_x^{(0)}=\int_{\Delta S}n_x^{(0)}\mathrm{d}s$ from the GB itself and other transverse noise photon fluxes $N_{x(\text{other})}^{(0)}=\int_{\Delta S}n_{x(\text{other})}^{(0)}\mathrm{d}s$ from thermal noise sources, blackbody radiation, and other secondary noise terms [41] caused by BPF. Since $N_x^{(1)}$ is often accompanied simultaneously by $N_{x(\text{noise})}^{(0)}$, in order to display $N_x^{(1)}$, $N_x^{(1)}\Delta t$ must be larger than the total noise photon flux fluctuation $\sqrt{N_{x(\text{noise})}^{(0)}\Delta t}$, *i.e.*, the displaying condition is given by

$$N_x^{(1)}\Delta t>\sqrt{N_{x(\text{noise})}^{(0)}\Delta t}$$

and

$$\Delta t>\frac{N_{x(\text{noise})}^{(0)}}{\left(N_x^{(1)}\right)^2}=\Delta t_{\min} \tag{C4}$$

where $\Delta t_{\min}$ is the requisite minimal accumulation time of the signal to overcome noise photon flux. Except for $N_x^{(0)}$, the major fraction of $N_{x(\text{noise})}^{(0)}$ is from diffraction noise, thermal noise, etc. Under a low-temperature, hard-vacuum operation and special geometric combination condition, the contribution to $N_{x(\text{noise})}^{(0)}$ is often less than $N_x^{(0)}$ [42].

Leveraging these important properties and employing the latest in technology [41]-[46], the 3DSR may obtain record HFGW sensitivity, and there is significant room for improvement to approach the required detection conditions (see **Table C1**).

Table C1. The transverse signal photon flux $N_x^{(1)}$ and allowable upper limits of transverse noise photon flux $N_{x(\text{noise})}^{(0)}$. According to the calculation of $N_x^{(1)}$, $N_x^{(0)}$ and other secondary noise photon fluxes $N_{x(\text{other})}^{(0)}$ in Ref. [44], $N_x^{(1)} = \int_{\Delta S} n_x^{(1)} \mathrm{d}y\mathrm{d}z$, $N_{x(\text{other})}^{(0)} = \int_{\Delta S} n_{x(\text{other})}^{(0)} \mathrm{d}y\mathrm{d}z$, $N_x^{(0)} = \int_{\Delta S} n_x^{(0)} \mathrm{d}y\mathrm{d}z$, where $\Delta S \approx 3\times 10^{-2}\ \mathrm{m}^2$. We list numerical results for $N_x^{(1)}$, $N_x^{(0)}$ and $\Delta t_{\min}$ in **Table C1**. Notice that transverse background photon flux vanishes at the longitudinal symmetrical surface, *i.e.*, $N_x^{(0)}\big|_{x=0} \equiv 0$. Thus, once the amplitude of HFGW and $\Delta t_{\min}$ are determined, an allowable upper limit of $N_{x(\text{noise})}^{(0)}$ is determined (see Equation (4)).

h	$N_x^{(1)}\left(\mathrm{s}^{-1}\right)$	$\Delta t_{\min}(\mathrm{s})$	Allowable Upper Limit of $N_{x(\text{noise})}^{(0)}\left(\mathrm{s}^{-1}\right)$
10^{-25}	2.6×10^{7}	3.0×10^{5}	$\sim 2.0\times 10^{20}$
10^{-27}	2.6×10^{5}	3.0×10^{5}	$\sim 2.0\times 10^{16}$
10^{-30}	2.6×10^{2}	3.0×10^{6}	$\sim 2.0\times 10^{11}$

(C.3.2.1) The transverse photon flux passing through the longitudinally symmetrical surface ($x = 0$).

If we let $X = 0$ be the surface having zero transverse BPF, *i.e.*, $N_x^{(0)}\big|_{x=0} \equiv 0$ while then numerical calculation shows that $N_x^{(1)}\big|_{x=0}$ has a maximum [29]. This means that any photon measured from $N_x^{(1)}|_{x=0}$ is a signal of EM perturbation produced by relic HFGW and is polarization sensitive (see **Figure C3**).

Table C1 shows that if Ω_{gw} of relic HFGWs expected by the pre-big-bang model can reach up its upper limit 6.9×10^{-6} [32], then $h \approx 1.0\times 10^{-30}$ at $v_g = 2.9$ GHz, and $N_x^{(1)}\big|_{x=0} \approx 2.6\times 10^{2}\ \mathrm{s}^{-1}$. This means that relic HFGW will leave a signature within the signal photons of $\sim 7.8\times 10^{8}$ in the signal accumulation time of 3×10^{6} seconds. Here $N_{x(\text{noise})}^{(0)}$ has a certain uncertainty in permitted values. However, because $N_x^{(0)}\big|_{x=0} \equiv 0$ and $N_{x(\text{noise})}^{(0)}$ are from secondary noise caused by the BPF, according to Equation (C4), the requirement of the allowable upper limit of 2.0×10^{11} for $N_{x(\text{noise})}^{(0)}$ passing through the symmetrical surface is possible

for the required sensitivity.

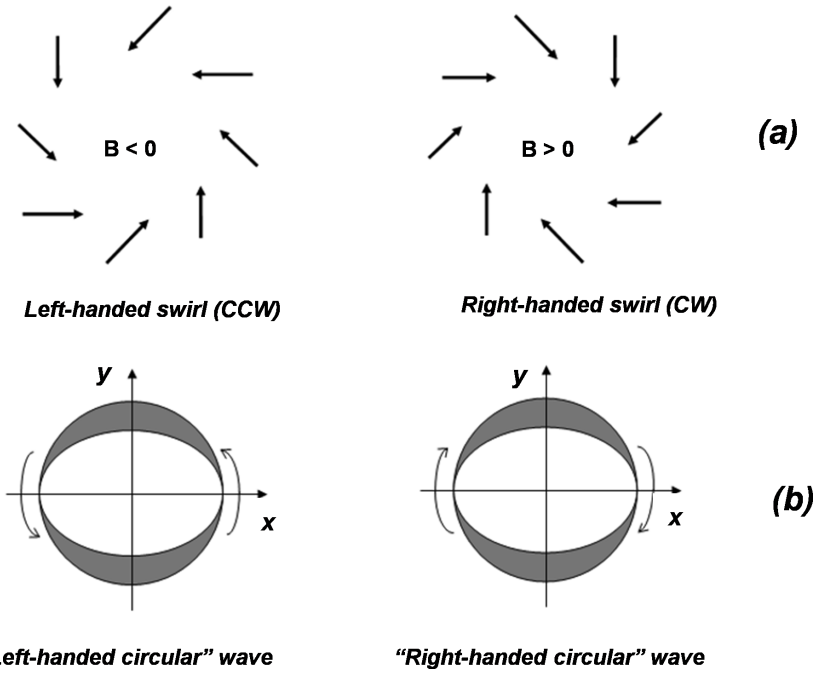


Figure C3. The polarization patterns in the CMB generated by the relic GWs are the left-handed and right-handed swirls, and only the GWs can produce the swirl patterns (divergence-less B-mode) (**Figure C3(a)**) [20]. On the other hand, the tangential distribution of the strength of perturbative photon flux generated by the HFGWs in the 3DSR is expressed as the "left-handed circular wave" and the "right-handed circular wave" [3], and only the GWs can generate these strength distribution patterns. Thus, direct detection of relic GWs in the high-frequency window (**Figure C3(b)**) and the indirect observation in the low-frequency window (**Figure 2**) would be complementary.

(C.3.2.2) The signal photon flux and the background photon flux in the "far-field detection-axis region".

When away from the symmetrical surface, $N_x^{(0)}$ will be a non-vanishing transverse BPF and will be a dominating transverse noise photon flux. For the HFGW parameters $h=10^{-30}$, $v_g=2.9\ \text{GHz}$, $N_x^{(1)}$, $N_x^{(0)}$ will have different decay rates and will reach up to a comparable order of magnitude at $x\sim 30\ \text{cm}$. Data in **Table A1** indicate that the best receiving surface for transverse photon flux is the longitudinal symmetrical surface, though it is immersed in the longitudinal background noise photon flux $n_z^{(0)}$. However, $n_z^{(0)}$, $n_x^{(0)}$ and $n_x^{(1)}$ are vectors, which have high directivity. The BPF generates thermal noise photons and other secondary noise photons in the FM focusing element. However, the BPF and noise photons have an essential difference. The former is a vector and has high directivity. Under conditions of low temperature, high vacuum, and shielding of the diffraction sources, the contribution of the latter to transverse photon flux will be less than the former.

The SQL defines the lower sensitivity limit for all measurements, including detection of the HFGWs [38]. It was shown [38] that the sensitivity limits $h_{\min}$ of

the 3DSR are obviously less than 10^{-30}. Thus, the predicted sensitivity limit in the 3DSR would be the photon signal limit, not the quantum noise limit.

C.4. Looking Ahead to the Future: Detecting and Observing Laboratory-Generated HFGWs

Direct detection and indirect measurement of laboratory-generated HFGWs in different frequency bands will provide definitive evidence of lab-generated HFGWs. By comparison, **Figure C4** shows the upper limit of energy density of relic GWs expected by cosmological models, showing possible utility to GW astronomy.

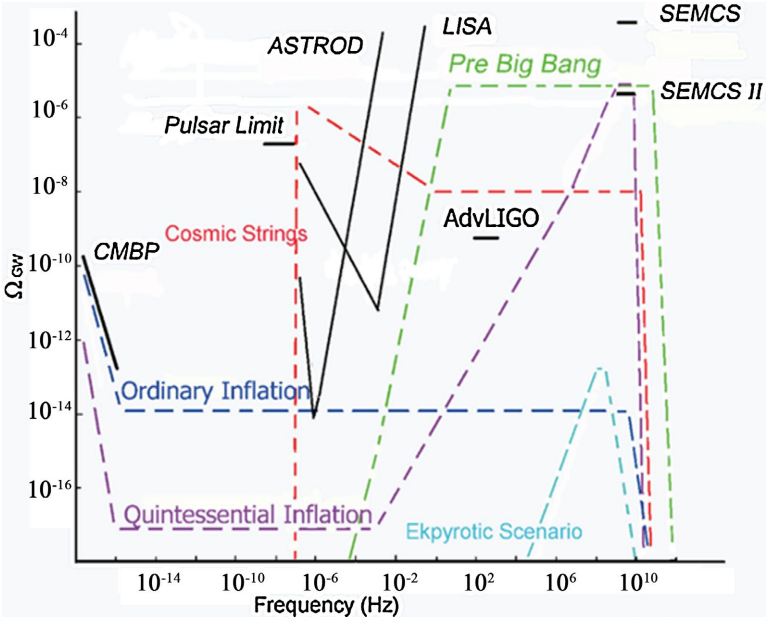


Figure C4. The upper limit Ω_{gw} expected by the typical cosmological models and possible detection means and observation ways. The Ω_{gw} curves are taken from Refs. [5] [8] [21]-[23] [32] [35] [47]-[50]. They show that Advanced LIGO will have sufficient sensitivity to directly detect the relic GWs at frequencies around 100 Hz in the pre-big-bang and in the cosmic string models. "SMECS" in this figure stands for detectors with "synchro-resonance electromagnetic coupling schemes", a class to which the 3DSR detector would belong.